Diffusion-driven instabilities by immobilizing the autocatalyst in ionic systems

Ágota Tóth[1] and Dezső Horváth[2, a)]

[1)] *Department of Physical Chemistry and Materials Science, University of Szeged, Aradi vértanúk tere 1., Szeged, H-6720, Hungary*

[2)] *Department of Applied and Environmental Chemistry, University of Szeged, Rerrich Béla tér 1., Szeged, H-6720, Hungary*

(Dated: 7 May 2015)

Spatiotemporal coupling of an autocatalytic chemical reaction between ions with diffusion yields various types of reaction-diffusion patterns. The driving force is short range activation and long range inhibition which can be achieved by selective binding of the autocatalyst even for ions with equal mobility. For Turing and lateral instability we show that identical charge on the autocatalyst and its counter part has a stabilizing effect on the base state, while opposite charge on them favors the formation of spatial patterns with reversible binding.

[a)] E-mail: horvathd@chem.u-szeged.hu

Self-organized spatial patterns may arise from the coupling of an autocatalytic chemical system with diffusion characterized by short range activation and long range inhibition. Simplest scenarios include Turing patterns and cellular fronts, both of which can not only be found in chemical systems but also appear in living organisms. In most cases ions are involved which may influence the underlying instability especially in biological examples where large molecules, like proteins, carry charges and act as polyelectrolytes, and yet their contribution is often neglected in theoretical works. When concentration gradients exist in reactions between ionic species, local electric field evolves allowing an additional transport for charged species unless high ionic strength is maintained. As a result, the flux of an ion will depend on the gradient of all ions present. When the spatial decoupling is achieved by selective reversible binding of the autocatalyst, the local electric field has an effect on the dynamics of the system even if the key components have the same diffusion coefficient. Two general scenarios can be identified: opposite charge on the autocatalyst and its counterpart leads to migrational flux that favors spatial pattern formation, while identical charge on them has a stabilizing effect. The phenomenon is presented in two prototype reaction-diffusion systems: the Turing instability of a homogeneous steady state and the lateral instability of a planar reaction front.

I. INTRODUCTION

Diffusion-driven instabilities lead to the evolution of chemical patterns[1,2] that are characterized by various concentration gradients absent in the unstable base state. Although diffusion generally acts in the direction to minimize spatial fluctuations in concentration, when coupled with an autocatalytic reaction, it can amplify the ever present noise resulting in the local enrichment of a chemical species.[3] The underlying driving force is differential diffusion with short range activation and long range inhibition, i.e., in these systems the autocatalyst has to diffuse at a slower rate than other key components.[4–7] Simplest scenarios of these diffusion-driven instabilities yield Turing patterns[8,9] and cellular fronts,[10,11] both of which can also appear in biological systems.[12–17]

When the autocatalytic reaction involves ions, migration represents an additional form of transport.[18] In these systems electric field therefore has a strong effect on the pattern formation, as shown by several theoretical[19,20] and experimental[21–24] works. Unless a high ionic strength is maintained by adding a conducting salt in large concentration,[25] local electric field arises due to the difference in the mobility and concentration of the various ions. Since all ions with concentration gradient contribute to the potential gradient, the flux of a single ion will also depend on the gradient of other ions. This, in effect, is similar to cross-diffusion, the effect of which has also been studied recently.[26,27]

Although experimental studies of pattern formation have mainly considered reactions between ions, the effect of charge on the species has most often been neglected. For simple two-component systems we have shown[28] that identical charge on the key species stabilizes, while opposite charges destabilize the base state, thus the latter scenario requires smaller difference between the diffusion coefficients for the onset of instability. This statement holds for both Turing patterns developing from unstable homogeneous states and cellular fronts replacing planar reaction fronts.

In experimental realization of diffusion-driven patterns, the biggest challenge is to achieve the desired difference in diffusion coefficients. The simplest chemical reactions are run in aqueous solution where all small hydrated ions diffuse at about the same rate with the exception of hydrogen and hydroxide ions. Successful approaches have involved the selective binding of the autocatalyst in order to decrease its effective diffusion coefficient: starch has been used for binding triiodide,[29,30] cyclodextrin for iodide,[4] carboxylate groups in a polymer chain for hydrogen ion[5–7,31–34]. Lengyel and Epstein in a series of papers[35–37] have shown that the binding of the autocatalyst into an immobile species in fact represents a shift in the time scale of the autocatalyst, since it also acts on the kinetic term. In the chlorite–iodide–malonic acid reaction the presence of starch suppresses the homogeneous oscillations by shifting the Hopf-bifurcation allowing the formation of Turing patterns. The same approach in simple autocatalytic reaction fronts has led to the lowering of the free autocatalyst concentration behind the front,[31,38] through which the flux of the autocatalyst decreases at the reaction zone allowing the destabilizing flux of the reactant to dominate and therefore leads to the appearance of cellular fronts.

In this work we show how the charge on the key species will affect the diffusion-driven instabilities in systems where the autocatalyst and its counterpart diffuse at the same rate

as they have the same mobility, and only selective binding of the autocatalyst is applied. Of spatial pattern formation we select two general scenarios: the Turing instability of a homogeneous state and the lateral instability of planar autocatalytic fronts. Charged versions of the Schnakenberg model[39] are used for the former and those of the cubic autocatalysis for the latter as prototypes. The key interest here is how the system behaves when the autocatalyst and its counterpart have the same or the opposite charge. We present first the governing equations and the characteristics of the selective binding via a fast equilibrium, then introduce the models and the obtained results separately. At the end we summarize the general features of the selective binding in ionic systems.

II. REACTION-DIFFUSION-MIGRATION MODEL

We consider systems where a chemical reaction occurs between aqueous ions and the only transport processes are diffusion and migration. The general component balance equation based on the Nernst-Planck equation takes the form of

$$\frac{\partial C_i}{\partial t} = D_i \nabla^2 C_i + \frac{z_i F D_i}{RT} \nabla (C_i \nabla \Psi) + \mathcal{F}_i(C_1, \ldots, C_n) \ , \tag{1}$$

where C_i is the concentration and z_i is the charge of the ith component with diffusion coefficient D_i, and $\mathcal{F}_i$ is the term representing the reaction kinetics. In Eq. (1) the Einstein relation $\mu_i = z_i F D_i/(RT)$ is applied to express ionic mobility. The charge balance

$$\frac{\partial Q}{\partial t} = \sum_{i=1}^{n} z_i \frac{\partial C_i}{\partial t} = \sum_{i=1}^{n} \left(z_i D_i \nabla^2 C_i + \frac{z_i^2 F D_i}{RT} \nabla (C_i \nabla \Psi) \right) = 0 \tag{2}$$

has to be taken into account to complete the system, where no kinetic term appears, since charge is conserved in a chemical reaction, i.e., $\sum_{i=1}^{n} z_i \mathcal{F}_i = 0$. In Eq. (2) it is explicitly stated that no macroscopic charge separation occurs with $Q = \sum_{i=0}^{n} z_i C_i = 0$, which is the scenario in an aqueous solution under normal conditions. Although charge separation is indeed negligible, potential gradient does arise locally where significant change in the composition exists as a result of the difference in ionic mobility.

For convenience the dimensionless form of Eqs. (1) and (2) are addressed, where $c_i = C_i/C_{1,0}$ is the dimensionless concentration relative to the initial concentration of one of reactants selected arbitrarily, $\delta_i = D_i/D_1$ is the ratio of diffusion coefficients with respect to the selected species, and $\psi = \Psi F/(RT)$ is the dimensionless electric potential. In this

work we restrict our investigation to systems with equal diffusion coefficients, i.e., $\delta_i = 1$. Time is scaled as $\tau = t/t_c$, where t_c is the reciprocal of the pseudo-first-order rate constant associated with one of the steps in the reaction mechanism appearing in $\mathcal{F}_i$, and the new length scale is $\xi = x/\sqrt{D_1\, t_c}$.

III. REVERSIBLE BINDING OF THE AUTOCATALYST

The amount of free autocatalyst (X) in the system may be controlled by the addition of a binding species via the fast equilibrium

$$\mathrm{X} + \mathrm{M} \rightleftharpoons \mathrm{MX} \ , \tag{3}$$

where—in addition in spatial systems—M and hence MX have generally negligible diffusion rate. In experimental realization the binding species is either a large molecule or a cross-linked polymer. In the latter case M represents the monomer unit where the actual binding takes place. From the dissociation constant (K_d) of MX the total concentration of the autocatalyst may be expressed as

$$[\mathrm{X}]_T = [\mathrm{X}] + [\mathrm{MX}] = \left(1 + \frac{C_M}{[\mathrm{X}] + K_d}\right)[\mathrm{X}] \equiv \Sigma[\mathrm{X}] \ , \tag{4}$$

where Σ represents the ratio of total and free autocatalyst and C_M is the total concentration of the binder.[31] For the rate of change of concentrations we have

$$\frac{\partial[\mathrm{X}]_T}{\partial t} = \left(1 + \frac{C_M K_d}{([\mathrm{X}] + K_d)^2}\right)\frac{\partial[\mathrm{X}]}{\partial t} \equiv \sigma\frac{\partial[\mathrm{X}]}{\partial t} \ , \tag{5}$$

hence the binding shifts the time scale of the autocatalytic species with respect to the other components of the reaction. Since $\sigma > 1$, it leads to a decrease both in the flux of the autocatalyst by decreasing its gradient and in the source term determined by the chemistry. Two general scenarios have been applied in experimental systems. For weak binding when $K_d \gg [\mathrm{X}]$, a large excess of M provides an essentially constant value for $\sigma = 1 + C_M/K_d$. In case of strong binding on the other hand, a small amount of M is sufficient to control the binding of X with σ depending on the concentration of the autocatalyst: at low concentration of X effectively all autocatalyst produced in the reaction will be bound, while at higher concentrations σ tends to unity representing a minimal binding. We only consider scenarios where the concentration of binder (chared or uncharged) is small with respect to the solvent

and its mobility is negligible, therefore Eqs. (1) and (2) remain applicable in the presence of polyelectrolytes.

In the governing equations therefore only the one for the autocatalyst—labeled with index 2 throughout this paper—is affected by the binding, and hence in dimensionless form we have

$$\frac{\partial c_i}{\partial \tau} = \nabla^2 c_i + z_i \nabla \left(c_i \nabla \psi \right) + f_i(c_1, \ldots, c_n) \quad i \neq 2 \ , \tag{6a}$$

$$\frac{\partial c_2}{\partial \tau} = \frac{1}{\sigma} \left(\nabla^2 c_2 + z_2 \nabla \left(c_2 \nabla \psi \right) + f_2(c_1, \ldots, c_n) \right) \tag{6b}$$

with $\sigma = 1 + \dfrac{c_M \, K}{(K + c_2)^2}$, $c_M = C_M / C_{1,0}$, and $K = K_d / C_{1,0}$, accordingly. At this stage it is important to point out that the differential charge balance equation is invariant to the presence of binding species because species M and MX are both immobile and inert, i.e., they neither diffuse and migrate nor take part in the rate laws given in $f_i = \mathcal{F}_i \, t_s / C_{1,0}$. Considering the charge balance, two general cases are addressed specifically. When M is neutral, X and MX have identical charges and therefore

$$Q = z_1 c_1 + z_2 \Sigma c_2 + \cdots + z_n c_n = 0 \quad \text{with} \quad z_M = 0 \tag{7}$$

with $\Sigma = 1 + \dfrac{c_M}{K + c_2}$ in dimensionless form, while with M having an opposite charge with respect to X, MX is neutral leading to

$$Q = z_1 c_1 + z_2 \Sigma c_2 + \cdots + z_n c_n - z_2 c_M = 0 \quad \text{with} \quad z_M = -z_2 \ . \tag{8}$$

Both Eqs. (7) and (8) yield the same equation

$$\frac{\partial Q}{\partial \tau} = z_1 \frac{\partial c_1}{\partial \tau} + z_2 \sigma \frac{\partial c_2}{\partial \tau} + \cdots + z_n \frac{\partial c_n}{\partial \tau} = 0 \tag{9}$$

for the rate of change. Since the factor σ appears in the sum above, it cancels out in the final dimensionless charge balance

$$\frac{\partial q}{\partial t} = \sum_{i=1}^{n} \left(z_i \nabla^2 c_i + z_i^2 \nabla (c_i \nabla \Psi) \right) = 0 \ . \tag{10}$$

IV. TURING INSTABILITY

The base state is the homogeneous state where the concentration gradients vanish, therefore we are faced with the solution of

$$f_i(c_1, \ldots, c_n) = 0 \ , \quad \psi = 0 \ . \tag{11}$$

The solution itself is independent of the extent of binding, as no σ appears in the time-independent problem. To investigate the stability of the homogeneous state, we introduce spatial perturbations, which we formulate in one spatial dimension without loss of generality as

$$c_i(\xi,\tau) = c_{i,0} + \sum_k c_{i,1,k}\phi(\xi,\tau) \ , \tag{12a}$$

$$\psi(\xi,\tau) = \sum_k \psi_{1,k}\phi(\xi,\tau) \ , \tag{12b}$$

where $c_{i,0}$ represents the homogeneous state, i.e. the solution of Eq. (11), ϕ_k is spatial perturbation with wave number k. In the linear stability analysis upon substituting into Eqs. (6) and (10), we only retain the terms linear in ϕ_k, the perturbation can therefore be expressed as $\phi_k = \exp(\omega\tau + ik\xi)$, with ω representing the temporal eigenvalue, also termed growth rate. The first order terms comprise the

$$\omega \begin{pmatrix} 1 & 0 & \dots & 0 & 0 \\ 0 & 1 & \dots & 0 & 0 \\ \dots & \dots & \dots & \dots & \dots \\ 0 & 0 & \dots & 1 & 0 \\ 0 & 0 & \dots & 0 & 0 \end{pmatrix} \begin{pmatrix} c_{1,1,k} \\ c_{2,1,k} \\ \dots \\ c_{n,1,k} \\ \psi_{1,k} \end{pmatrix} = M \begin{pmatrix} c_{1,1,k} \\ c_{2,1,k} \\ \dots \\ c_{n,1,k} \\ \psi_{1,k} \end{pmatrix} \tag{13}$$

generalized eigenvalue problem with Jacobian matrix

$$M = \begin{pmatrix} J_{1,1} - k^2 & J_{1,2} & \dots & J_{1,n} & -z_1 c_{1,0} k^2 \\ J_{2,1}/\sigma & (J_{2,2} - k^2)/\sigma & \dots & J_{2,n}/\sigma & -z_2 c_{2,0} k^2/\sigma \\ \dots & \dots & \dots & \dots & \dots \\ J_{n,1} & J_{n,2} & \dots & J_{n,n} - k^2 & -z_n c_{n,0} k^2 \\ -z_1 k^2 & -z_2 k^2 & \dots & -z_n k^2 & -\sum z_i^2 c_{i,0} k^2 \end{pmatrix} \ , \tag{14}$$

where $J_{i,j} = \partial f_i/\partial c_j$. When ω has a negative real part in the dispersion curve for all wave numbers, the homogeneous state is stable; any perturbations decay exponentially. For Turing instability to occur, ω should have a positive real part for some $k > 0$, i.e., the homogeneous state remains stable only towards homogeneous perturbations, in which case the unstable modes are amplified leading to a stationary heterogeneous concentration distribution once the nonlinear terms come into effect.

A. Model

We base our study on the Schnakenberg model[39]

$$\mathrm{A} \xrightarrow{\mathrm{k_1}} \mathrm{X} \tag{15a}$$

$$\mathrm{B} \xrightarrow{\mathrm{k_2}} \mathrm{Y} \tag{15b}$$

$$2\mathrm{X} + \mathrm{Y} \xrightarrow{\mathrm{k_3}} 3\mathrm{X} \tag{15c}$$

$$\mathrm{X} \xrightarrow{\mathrm{k_4}} \mathrm{P} \tag{15d}$$

$$\mathrm{MX} \overset{\mathrm{K}}{\rightleftharpoons} \mathrm{M} + \mathrm{X} \tag{15e}$$

in which A and B represent pool chemicals with constant concentrations and hence we are faced with a two-variable model. We consider two modifications of the model. In one we allow opposite charge for X and Y, leading to

$$\mathrm{A} \xrightarrow{\mathrm{k_1}} \mathrm{X^-} + \mathrm{E_2^+} \tag{16a}$$

$$\mathrm{B} \xrightarrow{\mathrm{k_2}} \mathrm{Y^+} + \mathrm{E_1^-} \tag{16b}$$

$$2\mathrm{X^-} + \mathrm{Y^+} \xrightarrow{\mathrm{k_3}} 3\mathrm{X^-} + 2\mathrm{E_2^+} \tag{16c}$$

$$\mathrm{X^-}(+\mathrm{E_2^+}) \xrightarrow{\mathrm{k_4}} \mathrm{P_1} \tag{16d}$$

$$\mathrm{E_1^-}(+\mathrm{E_2^+}) \xrightarrow{\mathrm{k_5}} \mathrm{P_2} \tag{16e}$$

$$\mathrm{MX} \overset{\mathrm{K}}{\rightleftharpoons} \mathrm{M^-} + \mathrm{X^+} \tag{16f}$$

where $\mathrm{E_1^-}$ and $\mathrm{E_2^+}$ are additional species introduced to account for the charge balance. In Eq. (16) parentheses indicate that the given species does not appear in the appropriate rate law, ensuring the same kinetic model. The reaction step in Eq. (16e) is included in order to have only neutral products in accordance with all schemes. In the other model we have identical charge on X and Y, hence

$$\mathrm{A} \xrightarrow{\mathrm{k_1}} \mathrm{X^-} + \mathrm{E^+} \tag{17a}$$

$$\mathrm{B} \xrightarrow{\mathrm{k_2}} \mathrm{Y^-} + \mathrm{E^+} \tag{17b}$$

$$2\mathrm{X^-} + \mathrm{Y^-} \xrightarrow{\mathrm{k_3}} 3\mathrm{X^-} \tag{17c}$$

$$\mathrm{X^+}(+\mathrm{E^+}) \xrightarrow{\mathrm{k_4}} \mathrm{P} \tag{17d}$$

$$\mathrm{MX} \overset{\mathrm{K}}{\rightleftharpoons} \mathrm{M^+} + \mathrm{X^-} \tag{17e}$$

where $\mathrm{E^+}$ is the extra charged species having the same role as $\mathrm{E_1^-}$ and $\mathrm{E_2^+}$ in Eq. (16).

For the calculation of the dispersion curves ($\omega - k$) the eigenvalue problem is solved by using the DGGEV routine (and the DGEEV routine for the neutral reference case) provided in LAPACK.[40] The original governing equations in Eqs. (6) and (10) are also integrated on a one-dimensional grid of 501 points and uniform $\Delta\xi = 0.1$ spacing and no-flux boundary conditions at each end with tolerance 10^{-8} using the CVODE package.[41] The parameter set is selected so that stable homogeneous oscillation exists for the reference neutral case with $k_1 a = 0.001$, $k_2 b = 0.01$, $k_3 = 2.57 \times 10^{-4}$, and $k_4 (= k_5) = 1.4$. For the binding $K = 0.01$ is fixed and c_M is varied.

B. Results

The oscillations present in the absence of binding can be suppressed by increasing the amount of binding species (M), which will decrease the concentration of the free autocatalyst. The stability against homogeneous perturbations is achieved via a Hopf-bifurcation at $k = 0$ on the dispersion curve as c_M is increased (see Fig. 1), with its value slightly depending on the binding strength as shown in Fig. 2. The stabilization of the homogeneous state, however, does not take place, since a range of unstable modes for $k > 0$ persists. This region is bounded by the marginal wave numbers where $\omega = 0$, which are invariant to the change in c_M because σ does not appear in the eigenvalue problem for $\omega = 0$. Although the width of the region of instability does not vary, the extent of binding with increasing c_M, and in effect σ, will decrease the temporal eigenvalue by shifting the time scale.

The location of the marginal wave numbers depends on the charges placed on the key species. As shown in Fig. 3, the lower bound $k_{0,1}$ is smaller, while the upper bound $k_{0,2}$ is greater for opposite charges on X and Y, widening the range of unstable modes. The opposite scenario occurs for identical charges on X and Y: $k_{0,1}$ is greater and $k_{0,2}$ is smaller than in the neutral case, therefore fewer modes remain unstable in the finite system. Comparison of the various models reveals that the effect of charged species is more pronounced when the binder itself is neutral, delivering the widest unstable region for opposite and strikingly shrinking range for identical charges, because the charged binder in a sense also acts as an ionic strength buffer.

Considering the change in the most unstable mode as the extent of binding is increased, Fig. 4 indicates that beyond the Hopf-bifurcation the temporal eigenvalue decreases signifi-

cantly as the time scale changes due to the increase in c_M and hence σ, while the shift in the wave number associated with the mode is insignificant. Comparing the different models, we can state that the mode is more unstable with greater ω_m for systems with opposite charge on X and Y, while it is less unstable with identically charged X and Y. The deviations from the neutral reference case is more pronounced with natural binder M, which can even lead to complete stabilization of the homogeneous state rapidly as ω_m changes its sign to negative at $c_M = 0.2828$.

Since there is a range of unstable spatial modes even before we reach the Hopf-bifurcation on increasing c_M, stable Turing patterns can also evolve from the perturbed homogeneous state for $c_M < c_{M,HB}$ when the limit cycle for homogeneous oscillations is still stable. In the reference neutral case as c_M is increased from 0.12 to 0.15, Turing pattern replaces the homogeneous temporal oscillation from the randomly perturbed base state. Opposite charge on X and Y increases the basin of attraction for Turing patterns, as they already form at $c_M = 0.12$, whereas identical charge on X and Y delays the appearance of Turing pattern until $c_M > 0.18$.

The final stable patterns are characterized by concentration distributions that strongly depend on the charges placed on the key components. Figure 5(a) reveals that there is a small shift in the wavelength: $\lambda = 7.41$ with identical charge on X and Y, while $\lambda = 6.25$ with opposite charge, which brackets the value associated with the neutral reference case ($\lambda = 6.67$). At the same time there is a striking difference between the phase of the spatial oscillations: for identical charges the concentration of X and Y varies out of phase with X having a maximum where Y is in minimum, and vice versa, similarly to the neutral reference case. For opposite charges the concentrations change in phase. This can be understood by realizing that a significant diffusion potential builds up in the system, as shown in 5(b), which leads to migrational fluxes in the opposite direction for X and Y when they have opposite charge, even though their concentration gradients have the same sign.

V. LATERAL INSTABILITY

The base state in this case is the planar reaction front propagating at a constant velocity (u) but expressed in a co-moving coordinate system to be defined as the time independent

solution of

$$0 = \frac{1}{\sigma_i}\frac{d^2c_i}{d\zeta^2} + u\frac{dc_i}{d\zeta} + \frac{1}{\sigma_i}\left[z_i\frac{d}{d\zeta}\left(c_i\frac{d\psi}{d\zeta}\right) + f_i(c_1,\ldots,c_n)\right] \ , \tag{18a}$$

$$0 = \sum_{i=1}^{n}\left[z_i\frac{d^2c_i}{d\zeta^2} + z_i^2\frac{d}{d\zeta}\left(c_i\frac{d\psi}{d\zeta}\right)\right] \ , \tag{18b}$$

where $\zeta = \xi - u\tau$ with ξ being the spatial coordinate in the direction of front propagation. The boundary conditions are set for this two-point boundary problem with only reactants ahead of the front ($\zeta \to +\infty$) and the products behind ($\zeta \to -\infty$). Unlike in the base state for Turing instability, the solution depends on the binding with σ remaining in Eq. (18). We expand the system in the second spatial coordinate without loss of generality and allow transverse perturbation in the front position $\zeta_p(\eta,\tau) = \sum_k \phi_k$, which leads to

$$c_i(\zeta,\eta,\tau) \ = \ c_{i,0}(\zeta) + \sum_k c_{i,1,k}(\zeta)\phi_k(\eta,\tau) \ , \tag{19a}$$

$$\psi(\zeta,\eta,\tau) \ = \ \psi_0(\zeta) + \sum_k \psi_{1,k}(\zeta)\phi_k(\eta,\tau) \ , \tag{19b}$$

where $c_{i,0}(\zeta)$ and $\psi_0(\zeta)$ represent the concentration and potential profile of the planar front, i.e, the solution of Eq. (18); ϕ_k is the spatial perturbation with wave number k. In the linear stability analysis, having expressed Eqs. (6) and (10) in the moving coordinate system and substituting Eq. (19) in, we only retain the terms linear in ϕ_k, the perturbation can therefore be expressed as $\phi_k = \exp(\omega\tau + ik\xi)$, with ω again representing the temporal eigenvalue. The spatial modes decouple and the generalized eigenvalue problem has now the form of

$$\begin{aligned}\omega c_{i,1,k} = {} & \frac{d^2c_{i,1,k}}{d\zeta^2} + u\frac{dc_{i,1,k}}{d\zeta} + z_i\left(\frac{dc_{i,0}}{d\zeta}\frac{d\psi_{1,k}}{d\zeta} + \frac{dc_{i,1,k}}{d\zeta}\frac{d\psi_0}{d\zeta} + c_{i,1,k}\frac{d^2\psi_0}{d\zeta^2} + \right. \\ & \left. c_{i,0}\frac{d^2\psi_{1,k}}{d\zeta^2}k^2c_{i,0}\psi_{1,k}\right) - k^2c_{i,1,k} + g_{i,k} \ ,\end{aligned} \tag{20a}$$

$$\begin{aligned}0 = \sum_{i=1}^{n}\Bigg[& z_i\left(\frac{d^2c_{i,1,k}}{d\zeta^2} - k^2c_{i,1,k}\right) + z_i^2\left(\frac{dc_{i,0}}{d\zeta}\frac{d\psi_{1,k}}{d\zeta} + \frac{dc_{i,1,k}}{d\zeta}\frac{d\psi_0}{d\zeta} + \right. \\ & \left. c_{i,1,k}\frac{d^2\psi_0}{d\zeta^2} + c_{i,0}\frac{d^2\psi_{1,k}}{d\zeta^2} - k^2c_{i,0}\psi_{1,k}\right)\Bigg] \ ,\end{aligned} \tag{20b}$$

where

$$g_{i,k} \ = \ \sum_j J_{i,j}c_{j,1,k} \ . \tag{21}$$

A. Model

The simplest autocatalytic model that exhibits lateral instability,[10] the cubic autocatalysis, is selected with formal kinetics according to

$$\mathrm{A} + 2\mathrm{B} \xrightarrow{\mathrm{k_c}} 3\mathrm{B} \tag{22a}$$

$$\mathrm{MB} \overset{\mathrm{K}}{\rightleftharpoons} \mathrm{M} + \mathrm{B} \tag{22b}$$

For studying the effect of charge we keep the kinetics unchanged and introduce opposite charge for A and B as

$$\mathrm{A}^- + 2\mathrm{B}^+ \xrightarrow{\mathrm{k_c}} 3\mathrm{B}^+ + \mathrm{C}^{2-} \tag{23a}$$

$$\mathrm{MB} \overset{\mathrm{K}}{\rightleftharpoons} \mathrm{M}^- + \mathrm{B}^+ \tag{23b}$$

where C^{2-} appears to account for the charge balance. For identical charge on A and B, we consider two scenarios: one where the ionic strength increases as more ions are produced according to

$$\mathrm{A}^- + 2\mathrm{B}^- \xrightarrow{\mathrm{k_c}} 3\mathrm{B}^- + \mathrm{C}^+ + \mathrm{D}^- \tag{24a}$$

$$\mathrm{MB} \overset{\mathrm{K}}{\rightleftharpoons} \mathrm{M}^+ + \mathrm{B}^- \tag{24b}$$

with C^+ and D^- being the chemically inert counterions, and the other with no change in the ionic strength as A is simply converted into B by

$$\mathrm{A}^- + 2\mathrm{B}^- \xrightarrow{\mathrm{k_c}} 3\mathrm{B}^- \tag{25a}$$

$$\mathrm{MB} \overset{\mathrm{K}}{\rightleftharpoons} \mathrm{M}^+ + \mathrm{B}^- \tag{25b}$$

Equation (18) is solved by using a relaxation method with the CVODE package on a grid of 801 points equally spaced ($\Delta\zeta = 0.25$). Exponential functions are applied for the concentrations as boundary conditions at both ends where the exponents are derived from the stability analysis of the limits at $\pm\infty$, which appear as steady states in the (c_i, $dc_i/d\zeta$) phase space. During the numerical integration of Eq. (18), the velocity of propagation u is reevaluated by using the formula

$$u = \int_{-\infty}^{+\infty} c_1 c_2^2 \, d\zeta \ , \tag{26}$$

the integral of Eq. (18a) for $i = 1$. The spatial discretization transforms the differential equations in Eq. (20) into a set of linear equations with a banded Jacobian matrix. The

DGGEV routine is applied to calculate the eigenvalues. To construct the dispersion curve, we trace the eigenvalue that evolves from the origin as k increases, since the $k = 0$ mode corresponds to the translation in the direction of propagation, for which the system is invariant, i.e., $\omega = 0$.

B. Results

With $c_M = 0.5$ the binding decreases the concentration of the free autocatalyst behind the reaction front to the extent so that its flux will be sufficiently smaller than that of the reactant. This destabilizes the planar reaction front indicated by the dispersion curve, allowing positive temporal eigenvalues for a range of wave numbers. On comparing the various models at this level of binding, we note that with opposite charges on A and B, the system is more unstable with respect to the neutral reference case. As shown in Fig. 6, the corresponding dispersion curve runs above that of the original system, providing a wider range of unstable modes and greater growth rates. Although the same concentration of autocatalyst develops behind the front independently of the charges, a positive electric field builds up ahead of the front (see Fig. 7), which enhances the destabilizing flux of reactant into the thin reaction zone. As a result, smaller binder concentration is sufficient to maintain the necessary difference in the fluxes, therefore the onset of lateral instability occurs at lower c_M.

With identical charge on A and B, a negative electric field develops ahead of the front (see Fig. 7), which decreases the flux of the reactant and hence has a stabilizing contribution. If the ionic change increases in the reaction according to Eq. (24), this stabilization is only partial: the dispersion curve runs below that of the neutral system but a range of unstable modes exists as shown in Fig. 6. This also means that the onset of instability occurs at greater extent of binding, since the flux of free autocatalyst with stabilizing effect has to be further decreased.

In the model with no change in the ionic strength, where A is simply converted into B (see Eq. (25)), the local electric field arising is so strong that complete stabilization is achieved. The growth rate (ω) remains negative for all $k > 0$ according to Fig. 6, characterizing a stable planar reaction front.

The results shown in Figs. 6 and 7 are obtained with M having an opposite charge with

respect to the autocatalyst, i.e., the immobile complex MB is neutral. When we set M to be neutral and use Eq. (7) instead of Eq. (8) for charge balance, we construct dispersion curves that runs above the appropriate ones shown in Fig. 6. The difference is greater for identical charge on A and B but even in that case the planar front remains stable for simple conversion of A into B according to Eq. (25a).

VI. DISCUSSION AND CONCLUSIONS

By investigating two prototype systems exhibiting diffusion-driven pattern formation—the Turing instability of a homogeneous state and the lateral instability of a planar reaction front—, we have shown that opposite charge on the autocatalyst and its counterpart favors the formation of spatial patterns, while identical charges have a stabilizing effect on the base state. This general behavior is therefore characteristics to systems where selective binding of the autocatalyst is applied even though the ionic species have equal diffusion coefficients and hence mobility. For Turing instability a binder without charge generally introduces greater stabilizing and destabilizing deviations, while for lateral instability it only has an additional destabilizing effect. Planar reaction fronts where the autocatalyst and the reactant have the same charge and no change in the ionic strength occurs remain stable even in the presence of selective binding.

The results confirm that the general tendency of stabilization with identical charges and destabilization with opposite charges is valid to systems not only with difference in diffusion coefficients but also with ions of equal mobility, provided selective binding is applied. In this case the shift in the time scale of the autocatalyst production is sufficient to spatially decouple it from the other components which is accompanied by the build-up of the local electric field. In general the flux of autocatalyst can also be decreased with the application of a a slowly diffusing binder with low mobility, which however represents a less effective scenario, since the transport of M and MX would lead to additional terms in Eq. (6).

In the experimental studies of this type of pattern formation, one has to remember that the charge of the species are determined by the selected system. With identical charge on the key components, the arising migrational flux will always have a stabilizing effect providing a smaller parameter space for instability to occur than in the hypothetical pure reaction-diffusion system. In reactions like that, the presence of an inert conducting salt would elim-

inate the local electric field and hence would widen the desired range of parameters. With opposite charges on the autocatalyst and its counterpart, we have an extra destabilizing effect in addition to the selective binding of the autocatalyst intrinsically, which may represent a parameter set experimentally more accessible for the observation of spatial patterns. The lateral instability of reaction fronts, for example, has first been shown in the iodate–arsenous acid[4] and the chlorite–tetrathionate reaction.[5,31] While in the latter the negative charge on the reactant and the positive charge on the autocatalyst lead to the additional destabilizing flux allowing large amplitudes in the cellular fronts with appropriate binding, the same charge in the former has the consequence of the very narrow parameter range resulting in cellular fronts with small amplitudes even though the applied pH buffer may have a contribution to the stucture by increasing the ionic strength. In redox reactions between anions with hydrogen ion being the autocatalyst, the opposite charges create a scenario that facilitates diffusion-driven pattern formation, and indeed systematic experimental studies have been successful in creating Turing patterns in acid-catalyzed chemical reactions.[6,42] With more complex system, especially where polyelectrolytes are present, migrational flux may even have more important contribution to spatiotemporal pattern formation.

ACKNOWLEDGMENTS

The authors dedicate this paper to Professor Irv Epstein on celebration of his 70th birthday for his outstanding contribution to nonlinear science. This work was financially supported by the Hungarian Scientific Research Fund (OTKA K84090) and TÉT.

REFERENCES

[1]I. R. Epstein and J. A. Pojman, *An Introduction to Nonlinear Dynamics: Oscillations, Waves, Patterns, and Chaos* (Oxford University Press, Oxford, 1998)

[2]C. Kapral and K. Showalter, *Chemical Patterns and Waves* (Kluwer, Dordrecht, 1995)

[3]A. Turing, Philos. Trans. Roy. Soc. London B **237**, 37 (1952)

[4]D. Horváth and K. Showalter, J. Chem. Phys. **102**, 2471 (1995)

[5]A. Tóth, I. Lagzi, and D. Horváth, J. Phys. Chem. **100**, 14837 (1996)

[6]J. Horváth, I. Szalai, and P. De Kepper, Science **324**, 772 (2009)

[7]M. Fuentes, M. N. Kuperman, and P. De Kepper, J. Phys. Chem. A **105**, 6769 (2001)

[8]A. De Wit, Adv. Chem. Phys. **109**, 435 (1999)

[9]T. Bánsági Jr., V. K. Vanag, and I. Epstein, Science **331**, 1309 (2011)

[10]D. Horváth, V. Petrov, S. K. Scott, and K. Showalter, J. Chem. Phys. **98**, 6332 (1993)

[11]Y. Kuramoto, "Dynamics of synergetic systems," (Springer, Berlin, 1980) p. 134

[12]S. Kondo and R. Asai, Nature (London) **376**, 765 (1995)

[13]A. Nakamasu, G. Takahashi, A. Kanbe, and S. Kondo, Proc. Natl. Acad. Sci. USA **106**, 8429 (2009)

[14]M. Mimura, H. Sakaguchi, and M. Matsushita, Physica A **282**, 283 (2000)

[15]Y. Shiferaw and A. Karma, Proc. Natl. Acad. Sci. USA **103**, 5670 (2006)

[16]E. Khain and L. M. Sander, Phys. Rev. Lett. **96**, 188103 (2006)

[17]S. Kondo and T. Miura, Science **329**, 1616 (2010)

[18]S. Schmidt and P. Ortoleva, J. Chem. Phys. **67**, 3771 (1977)

[19]A. Tóth, D. Horváth, and W. van Saarloos, J. Chem. Phys. **111**, 10964 (1999)

[20]Z. Virányi, Á. Tóth, and D. Horváth, J. Eng. Math. **59**, 229 (2007)

[21]Z. Virányi, Á. Tóth, and D. Horváth, Chem. Phys. Lett. **401**, 575 (2005)

[22]Z. Virányi, D. Horváth, and Á. Tóth, J. Phys. Chem. A **110**, 3614 (2006)

[23]H. Ševčíková and M. Marek, Physica D **9**, 140 (1983)

[24]H. Ševčíková and M. Marek, Physica D **13**, 379 (1984)

[25]Z. Virányi, A. Szommer, Á. Tóth, and D. Horváth, Phys. Chem. Chem. Phys. **6**, 3396 (2004)

[26]V. K. Vanag and I. R. Epstein, Phys. Chem. Chem. Phys. **11**, 897 (2009)

[27]M. A. Budroni, L. Lemaigre, A. De Wit, and F. Rossi, Phys. Chem. Chem. Phys. **17**,

1593 (2015)

[28]Z. Virányi, Á. Tóth, and D. Horváth, Phys. Rev. Lett. **100**, 088301 (2008)

[29]V. Castets, E. Dulos, J. Boissonade, and P. De Kepper, Phys. Rev. Lett. **64**, 2953 (1990)

[30]Q. Ouyang and H. L. Swinney, Nature (London) **352**, 610 (1991)

[31]D. Horváth and A. Tóth, J. Chem. Phys. **108**, 1447 (1998)

[32]I. Szalai and P. De Kepper, J. Phys. Chem. A **112**, 783 (2008)

[33]I. Szalai, J. Phys. Chem. A **118**, 10699 (2014)

[34]G. Csekő, L. Ren, Y. liu, Q. Gao, and A. K. Horváth, J. Phys. Chem. A **118**, 815 (2014)

[35]I. Lengyel and I. R. Epstein, Science **251**, 650 (1991)

[36]I. Lengyel and I. R. Epstein, Proc. Natl. Acad. Sci. USA **89**, 3977 (1992)

[37]I. Lengyel and I. R. Epstein, Acc. Chem. Res. **26**, 235 (1993)

[38]E. Jakab, D. Horváth, A. Tóth, J. H. Merkin, and S. K. Scott, Chem. Phys. Lett. **342**, 317 (2001)

[39]J. Schnakenberg, J. Theor. Biol. **81**, 389 (1979)

[40]E. Anderson, Z. Bai, C. Bischof, S. Blackford, J. Demmel, J. Dongarra, J. Du Croz, A. Greenbaum, S. Hammarling, A. McKenney, and D. Sorensen, *LAPACK Users' Guide* (Soc. for Industrial and Applied Mathematics, Philadelphia, 1999)

[41]S. D. Cohen and A. C. Hindmarsh, Comput. Phys. **10**, 138 (1996)

[42]H. Liu, J. A. Pojman, C. Pan, J. Zheng, L. Yuan, A. K. Horváth, and Q. Gao, Phys. Chem. Chem. Phys. **14**, 131 (2012)

Fig. 1 Dispersion curves for the reference neutral Schnakenberg model with increasing binding. Panel (a) shows the change in the real part of the growth rate because for small k the eigenvalues are complex numbers.

Fig. 2 The concentration of the binder at the Hopf-bifurcation for varying binding constant K. The homogeneous state is stabilized to homogeneous perturbations above these critical values of c_M, allowing the evolution of stable Turing patterns.

Fig. 3 The change in the lower (a) and the upper (b) marginal wave numbers with increasing binding for the differently charged systems relative to the invariant neutral reference system shown with dotted line.

Fig. 4 The change in the wave number (a) and the growth rate (b) of the most unstable mode with increasing binding for the differently charged systems. Dotted line shows the neutral reference system.

Fig. 5 The concentration (a) and the electric potential (b) profile of the stable Turing pattern characteristics for systems with identical (solid line) and opposite (dashed line) charge on the autocatalyst and its counterpart.

Fig. 6 Dispersion curves characterizing the planar fronts in the cubic autocatalysis with binding for variously charged reactant and autocatalyst.

Fig. 7 Electric field strength ($\epsilon = -d\psi/d\zeta$) arising in front of the reaction front for cubic autocatalysis with opposite (red line) charge on the reactant and the autocatalyst and identical charges with increasing (green line) and constant (blue lines) ionic strength. The $\zeta = 0$ coordinate indicates the location of maximum rate of reaction.

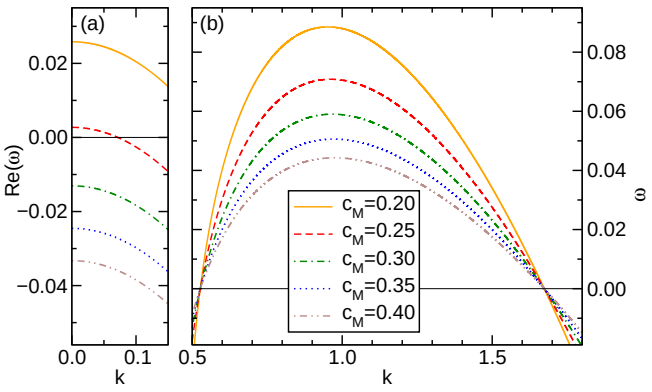

FIG. 1. Á. Tóth ... Chaos

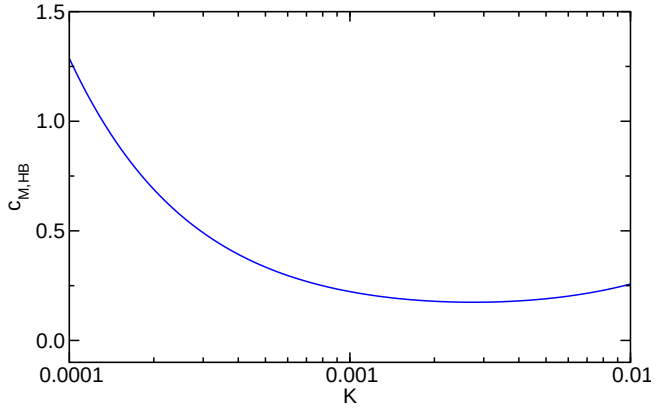

FIG. 2. Á. Tóth ... Chaos

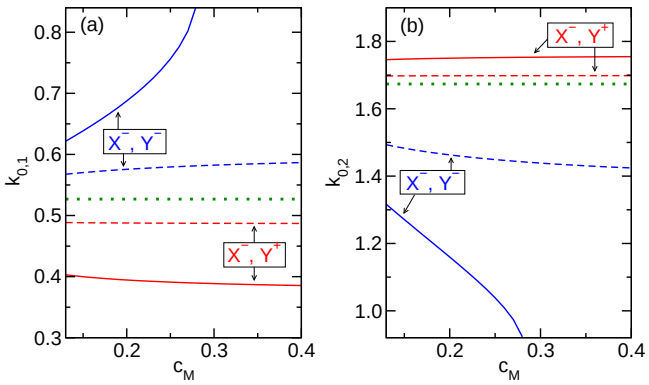

FIG. 3. Á. Tóth ... Chaos

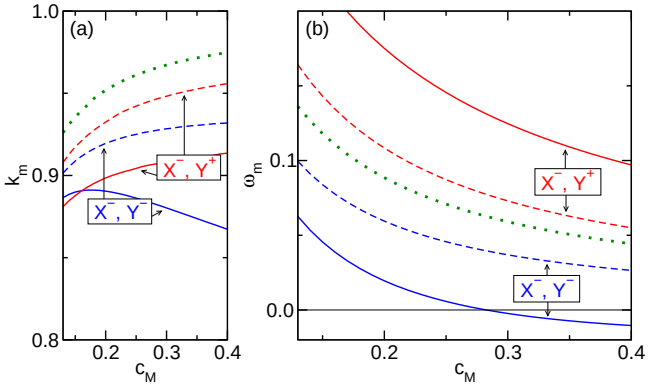

FIG. 4. Á. Tóth ... Chaos

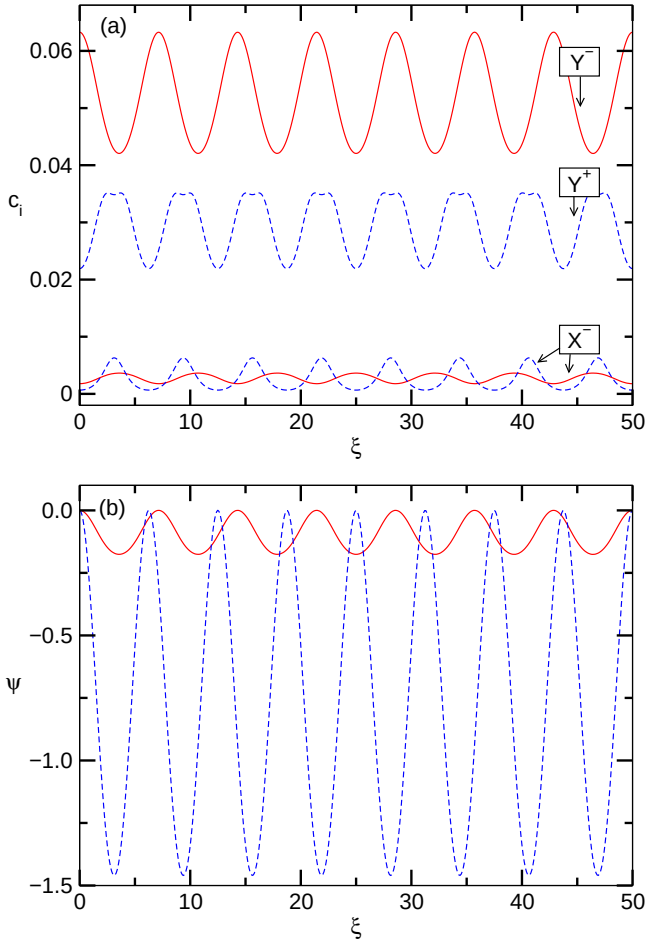

FIG. 5. Á. Tóth ... Chaos

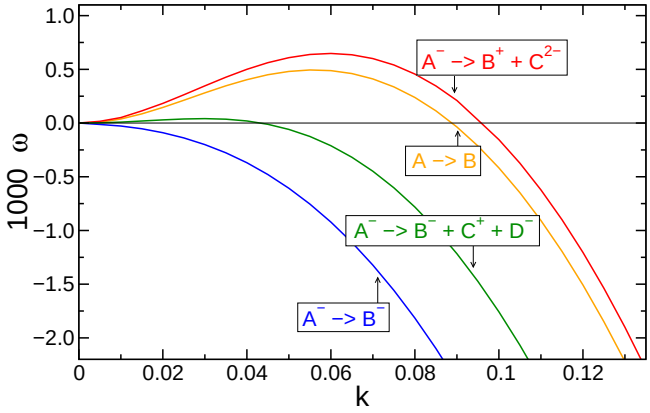

FIG. 6. Á. Tóth ... Chaos

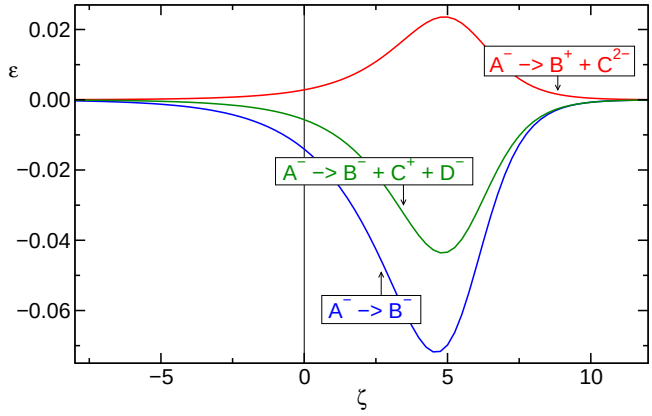

FIG. 7. Á. Tóth ... Chaos